4 Hunga effects on stratospheric temperatures and circulation

Lead authors Xinyue Wang
Lawrence Coy

Co-Authors Masatomo Fujiwara
Pu Lin
Alison Ming
Feng Li
Ewa M. Bednarz
Zhihong Zhuo
Kirstin Krüger

Contributing authors William Randel
Jon Starr
Wandi Yu
Simone Tilmes
Chengyun Yang
Yunqian Zhu
Jun Zhang
Simchan Yook
Eric Fleming
Peter Colarco
Shingo Watanabe
Mijeong Park
Martin Jucker

Cite this as:

Wang, X., L. Coy et al. (2025): Hunga effects on stratospheric temperatures and circulation. In APARC, 2025: The Hunga Eruption Atmospheric Impacts Report [Yunqian Zhu, Graham Mann, Paul A. Newman, William Randel (Eds.)]. APARC Report No. 11, WCRP Report No. 10/2025, DOI: 10.34734/FZJ-2025-05241, available at `https://aparc-climate.org/publications/aparc-report-no-11/`.

Key points

- The Hunga H_2O cloud, injected into the stratosphere in 2022, was spread globally by the residual mean circulation and lateral mixing along surfaces of constant potential temperature. The water vapour anomaly reached the polar region of each hemisphere after the breakdown of the Southern and Northern polar vortices in December 2022 and April 2023, respectively, and continues to persist over much of the stratosphere to the present (2025).

- The Hunga eruption led to a 0.5-1 K cooling of the global stratosphere in early 2022, which has extended through 2024. Larger temperature anomalies are observed in specific regions, but local Hunga impacts are entangled with dynamically forced variability.

- Cooling in the stratosphere is mainly due to radiative impact of the Hunga H_2O. The Hunga forced cooling contrasts to the stratospheric warming associated with aerosols in other major volcanic eruptions.

- The Southern Hemisphere winter stratospheric circulation was significantly disrupted following the Hunga eruption in 2022, with an unusually strengthened and equatorward shifted of the winter stratospheric jet, weakened residual mean circulation, and reduced planetary wave forcing. Models reproduce this observed behaviour but also exhibit significant internal variability of the same amplitude. Model simulations for spring 2023 show a wide range of Northern Hemisphere stratospheric responses, making it challenging to attribute changes to the Hunga eruption given the influence of internal variability.

- Observed temperature and circulation changes following Hunga eruption in the SH mid latitude stratosphere during the first austral winter are captured by global data assimilation systems. The MERRA-2 reanalysis, which assimilates MLS temperature observations above the 5-hPa level, follows best the MLS observations in and above the upper stratosphere. Without knowledge of the water vapour anomaly, these systems tracked Hunga induced changes in assimilated temperature observations, thus providing gridded global analysis of meteorological fields during 2022 and following years.

- Current pieces of evidence are insufficient to draw conclusions on whether the Hunga eruption affected the QBO, given the inconsistency between observations and the model simulations and the possible large internal variability in the system and the unrealistic QBO representation in the models.

Contents

4.1 The large-scale evolution of the Hunga H_2O cloud 92
4.2 Stratospheric transport, temperatures and zonal winds 92
4.2.1 Observations of temperature anomalies following the eruption of Hunga 92
4.2.2 Assimilated temperature and wind anomalies following the Hunga eruption 94
4.2.3 Hunga induced temperature and circulation anomalies in models 96
4.3 Residual mean meridional circulation and Eliassen-Palm flux 98
4.3.1 Residual mean meridional circulation and EP flux in the global data assimilation systems 98
4.3.2 Residual mean circulation and EP flux changes in models 99
4.4 Interaction of Hunga with the Quasi-Biennial Oscillation (QBO) 101
4.5 Summary 102

Preamble

The Hunga submarine volcano erupted on 15th January 2022 injected a massive plume of water vapour into the stratosphere. It increased the global stratospheric water burden by ~15% (Chapter 3), setting a record high for direct water vapour injection into the stratosphere in the modern satellite era and differentiating itself from previous major volcanic eruptions (Vömel et al., 2022; Khaykin et al., 2022). Most of the Hunga H_2O cloud then dispersed globally, remaining in the upper atmosphere through 2024 (Millán et al., 2022; Khaykin et al., 2022; Zhou et al., 2024). In addition to the water vapour, a moderate amount of sulfur-containing gas, equivalent to 0.5–1 Tg sulfur dioxide (SO_2), was lofted into the stratosphere by the Hunga eruption according to Carn et al. (2022), and converted to sulfate aerosol particles within one to two weeks (Zhu et al., 2022). After three months, the Hunga aerosol separated from the H_2O due to aerosol growth and sedimentation (Legras et al., 2022) and was mainly transported into the Southern Hemisphere (SH) lower stratosphere (Duchamp et al., 2023). Additional details on plume dispersion are discussed in Chapter 3. The large H_2O and aerosol perturbations affected stratospheric temperatures, circulation, and transport, as analysed in this chapter.

4.1 The large-scale evolution of the Hunga H_2O cloud

Satellite observations show that the Hunga H_2O plume has persisted in the stratosphere and evolved from 2022 through the end of 2024 (Millán et al., 2024). The global, latitude and altitude evolution of the Hunga H_2O anomaly followed the well-known residual mean (or Brewer-Dobson) circulation in the stratosphere (Figure 4.1). During January 2022, the initial volcanic cloud, near 20°S, 175°W, spread longitudinally around the globe with most of the water vapour anomaly remaining near the 20°S, 20 hPa (Figure 4.1a). The H_2O then spread laterally within the tropical pipe (Plumb, 1996), reaching 10 hPa by Feb 2022. It spread deep into the SH in December 2022, when the austral polar vortex broke down removing the mixing barrier. It then spread deeper into the Northern Hemisphere (NH) a few months later, in March, when its vortex broke down, removing mixing barriers in the north. Furthermore, by the start of 2023 the initial water vapour perturbation had been advected upward in the tropics and was now replaced by the typical dryer air through the tropopause (Figure 4.1b). Note that the upward motion at the equator was initially slow until June 2022.

4.2 Stratospheric transport, temperatures and zonal winds

4.2.1 Observations of temperature anomalies following the eruption of Hunga

Substantial stratospheric warming linked to enhanced aerosols has been observed following major volcanic eruptions such as El Chichón and Pinatubo (Labitzke and McCormick, 1992). However, the unprecedented H_2O perturbation after the Hunga eruption presents a distinct case in the observational record. Unlike sulfate aerosol, stratospheric water vapour acts as a greenhouse gas and is a strong emitter of longwave radiation, leading to localised cooling effect in the stratosphere (Sellitto et al., 2022). The dynamical variability and cooling trends in the stratosphere, along with the potential non-local dynamical effects from H_2O and aerosol clouds, make it challenging to isolate the stratospheric temperature impacts of the Hunga eruption. To address these complications, we have detrended the entire historical datasets from the Stratospheric Sounding Unit (SSU) channels and Microwave Limb Sounder (MLS) using regression fits based on the pre-Hunga period and additionally removed the influence of the 11-year solar cycle (Steiner et al., 2020; Randel et al., 2024). The Hunga-related temperature anomalies are compared to variability in the longer-term stratospheric climate record across several stratospheric layers over the modern satellite era in Figure 4.2. The time series in the stratosphere captures two distinct warming spikes in 1982 and 1991, corresponding to the El Chichón and Pinatubo volcanic eruptions. The warming in 2020 caused by the smoke injected from the Australian New Year's fires can also be seen (Rieger et al., 2021). Cooling effects from the Hunga eruption are noticeable in the middle to upper stratosphere during 2022–2023, with temperature residuals revealing anomalies of approximately -0.5 to -1 K throughout the stratosphere. The Hunga-related cooling is comparable in magnitude, though opposite in sign, to the warming anomalies associated with the El Chichón and Pinatubo eruptions. The sign difference is attributed to the intensified longwave cooling rate caused by the large amount of H_2O injected by Hunga (Wang et al., 2023; Wang and Huang, 2024; Gupta et al., 2025), as opposed to the sulfate aerosol-driven warming observed after El Chichón and Pinatubo. Additionally, the Hunga cooling anomalies increase substantially in magnitude from the lower to upper stratosphere into the meso-

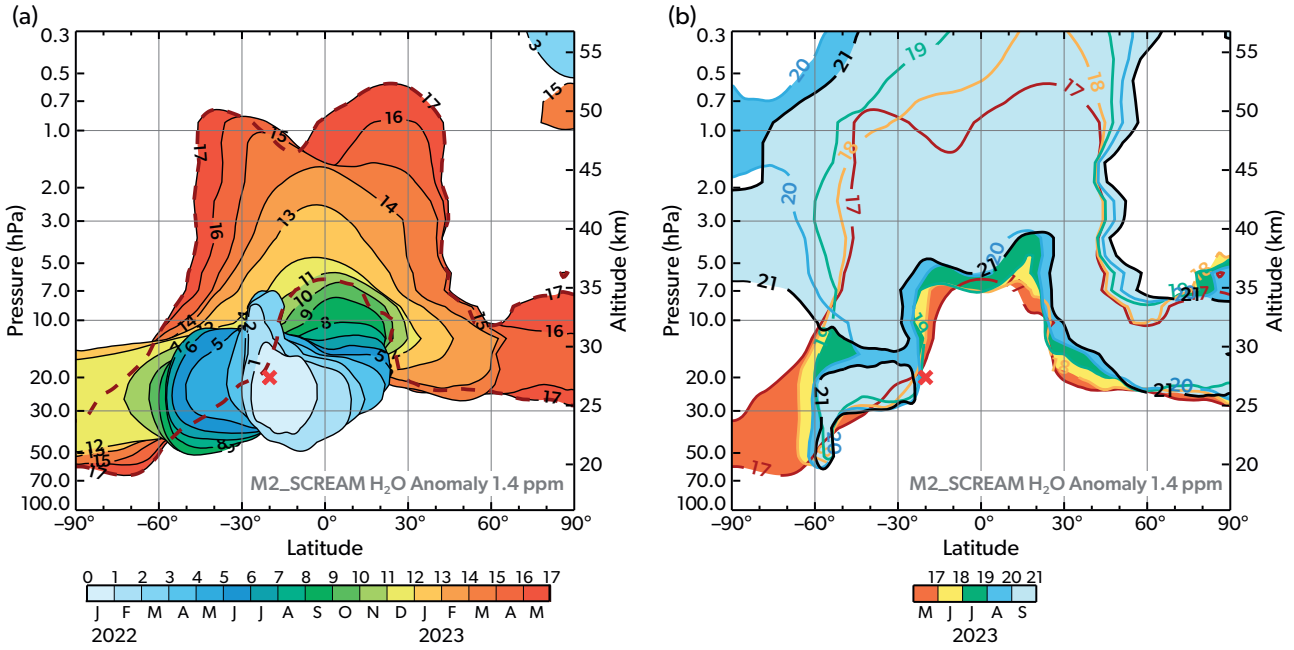

Figure 4.1: *Water vapour anomaly (1.4 ppm contour) plotted for each month starting at January 2022 (labelled 1) for a) January 2022 through May 2023, and b) May 2023 through September 2023. In a) the filled contours for earlier months are plotted on top of the later months, with the dashed curve being month seventeen.; in b) the filled contours for later months are plotted on top of the earlier months. The monthly averaged fields are taken from the MERRA-2 Stratospheric Composition Reanalysis of Aura Microwave Limb Sounder (M2-SCREAM), a global constituent data assimilation system. The red cross denotes the location 20°S, 20 hPa.*

sphere in response to ozone depletion (see discussion in Chapter 6), whereas the warming anomalies from El Chichón, Pinatubo, and the Australian wildfire peak in the lower stratosphere and decrease with altitude.

The systematic cooling influence of the Hunga eruption on global stratospheric temperatures is also evident in MLS observations. The global average MLS temperature anomalies as a function of altitude and time over 2022 to 2024 are presented in Figure 4.3. These anomalies are calculated as differences from the 2005–2021 MLS average after removing the decadal trends and natural variabilities via regression as discussed above. The black contour denotes the corresponding Hunga H_2O at 1 ppmv level. The H_2O cloud originated near 25–30 km in January 2022, with subsequent upward transport to the upper stratosphere and mesosphere by mid-2023. Cold anomalies of 0.5 K originated near 25–30 km two months after the eruption, coinciding with the altitude of the rising plume. During 2022 and 2023, cold temperature anomalies of ~0.5–1.0 K in the stratosphere closely aligned with the ascending Hunga H_2O, with slightly larger anomalies (~1.5–2.0 K) above ~45 km in the lower mesosphere after mid-2023. The vertical and temporal overlap of these temperature and H_2O anomalies provides strong evidence for the Hunga forcing on the observed temperature cooling. Gupta et al. (2025) quantified the radiative effects of stratospheric H_2O using satellite observations and radiative transfer simulations under clear sky conditions. Their results show that the Hunga H_2O caused a net radiative cooling rate of −0.15 K day^{-1} in the stratosphere in 2022, and a continued cooling of −0.1 K day^{-1} in 2023, consistent with our findings.

Notably, the mid-stratosphere experienced even more pronounced cooling in austral winter 2022. The global temperatures in the mid-stratosphere fell well below those recorded in previous years (Figure 4.4). These cold anomalies stood out one-to-two months after the eruption. This delay is consistent with a radiative response to the increased H_2O near this altitude, with a radiative damping time scale of ~10–20 days (Hitchcock et al., 2010). By July and August 2022, 20 hPa global temperatures were ~1 K below the multi-year average over 2005 to 2021. The cold anomalies persisted into 2023, becoming slightly weaker than in 2022 but remaining beyond the range of variability.

In the months following the eruption, both the water vapour and sulfur dioxide anomalies spread in latitude creating local temperature anomalies. Observed cold temperature anomalies and the H_2O plume over-

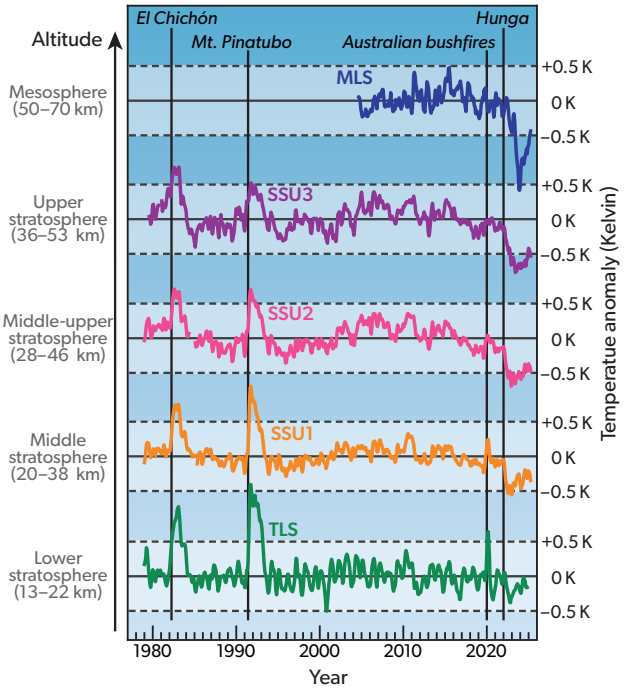

Figure 4.2: *Time series of monthly global average temperature anomalies for thick-layer averages spanning the lower to upper stratosphere (bottom to top). Linear trend and solar cycle fits have been subtracted. Lower stratosphere temperatures (TLS) are ~13-22 km layer averages from satellite microwave measurements. Middle and upper stratosphere data are from the SSU channels updated with microwave measurements, representing thick-layer averages centred near 30, 38 and 45 km (SSU1, SSU2 and SSU3, respectively). Mesospheric temperatures represent 50–70 km averages based on MLS data from 2005 to February 2025 (Randel et al., 2024). The four vertical dashed lines mark the timing of major events that caused stratospheric temperature anomalies: the eruptions of El Chichón (1982), Mount Pinatubo (1991), the 2019–2020 Australian wildfires, and the 2022 Hunga eruption. Adapted and updated from Randel et al. (2024).*

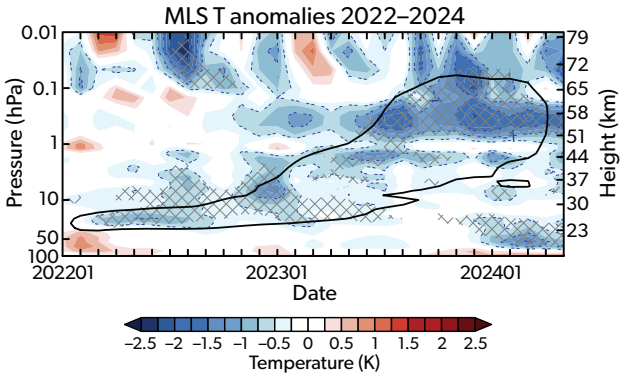

Figure 4.3: *Height and time sections of anomalous global average temperature anomalies (colour shadings) from MLS observations. Dashed blue contours indicate temperature anomalies at 0.5 K intervals. Solid black contour shows the location of Hunga H_2O plume at 1 ppmv level. The MLS observations have been detrended based on the entire MLS data (2005-2024) using fits derived from the pre-Hunga period (2004-2021) and the 11-year solar cycle, ENSO, and QBO variabilities have been removed using multilinear regression fits (adapted from Randel et al., 2024). The hatched regions are those evaluated as significant based on twice of the standard deviation of the anomalies for the period 2005-2021.*

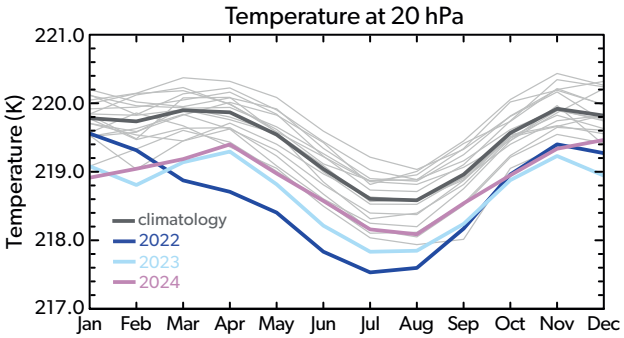

Figure 4.4: *Globally and monthly averaged temperatures at 20 hPa from the MLS observations showing persistent anomalous cooling since 2022. Gray lines show time series of MLS temperatures for 2005–2021 while the black line is the climatology. Navy/light-blue/purple lines show 20 hPa temperature for 2022/2023/2024, respectively.*

lapped until April (Figure 4.5a) and decoupled in early SH winter. In particular, 2022 austral winter months exhibited a striking cold anomaly in the mid latitudes of the SH, not directly overlapping the H_2O plume, as illustrated in Figure 4.5b. This significant cooling, in excess of 15 K in the mid-latitude upper stratosphere, is surprising in that much of it was located well above the water vapour anomaly, suggesting a non-local dynamical response to the volcanic perturbations. Part of the tropical and extratropical temperature maxima could be related to the phase of the QBO in 2022 (Coy et al., 2022). The temperature contrast between high and low latitudes is suggestive of a meridional shift of the zonal winds and associated changes in the mean meridional circulation (Yulaeva et al., 1994; Wang et al., 2023).

4.2.2 Assimilated temperature and wind anomalies following the Hunga eruption

Global atmospheric reanalyses are one of the fundamental data sets to understand atmospheric variability, and there are multiple reanalyses available, which sometimes show different results for the same diagnostic (SPARC, 2022). Here, we evaluate the influences of the Hunga eruption on stratospheric temper-

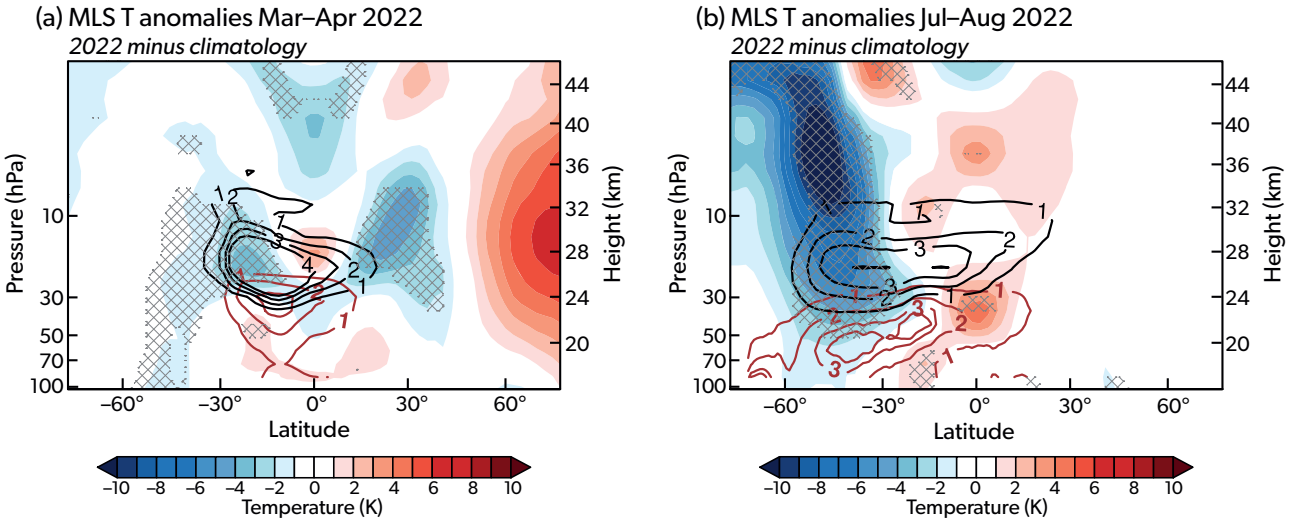

Figure 4.5: *MLS observed temperature anomalies averaged in (a) March and April and (b) July and August 2022 (colour shading, K), calculated as differences between the 2022 and the 2005–2021 average. Red line contours denote the sulfate aerosol extinction in 10^{-3} km^{-1}, and black line contours denote the anomalous H_2O concentration in ppmv. Hatched regions indicate where the 2022 anomalies are outside the range of all variability during 2005–2021 (Wang et al., 2023).*

ature and circulation across the global data assimilation (DA) systems, including MERRA-2 (Gelaro et al., 2017), JRA-3Q (Kosaka et al., 2024), ERA5 (with the period 2000–2006 replaced with ERA5.1) (Hersbach et al., 2020; Simmons et al., 2020), and JRA-55 (Kobayashi et al., 2015). Note that none of these reanalyses include the enhanced water vapour due to the Hunga eruption in the radiative transfer calculations in their forecast model. Thus, the temperature signals mainly come from various assimilated temperature observations. Coy et al. (2022) analysed MERRA-2 data and found that adjustments made during data assimilation compensated for the missing radiative cooling caused by the Hunga water vapour. This suggests that while the direct radiative impact of the eruption was not explicitly modelled, the resulting meridional circulation signals are likely realistic.

The temperature anomaly time series at 20 hPa at 45° S shows the strongest cooling in August 2022 following the Hunga eruption based on four reanalyses (Figure 4.6). These anomalies are calculated with respect to the 2005–2021 climatology. All four reanalyses track the temperature changes from month to month nearly identically, and all show negative anomalies after the Hunga eruption at 20 hPa, 45° S mid-stratosphere, with temperatures down to ~-8 K in the middle of 2022, comparing well with the MLS observation (Figure 4.5b).

For examination of changes at all latitudes and pressures, we focus on the months of July and August 2022, when the SH stratospheric polar vortex is strongest.

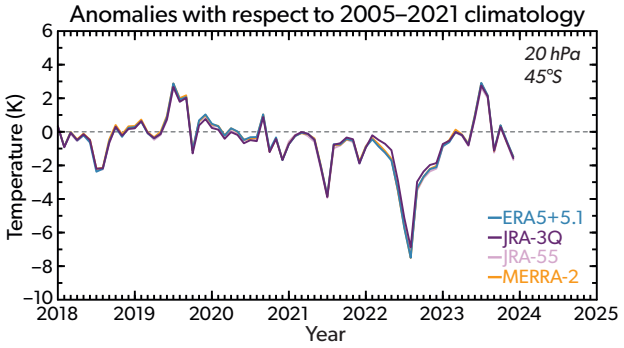

Figure 4.6: *Temperature anomaly times series at 20 hPa, 45°S for the four reanalyses. These anomalies are with respect to the 2005-2021 climatology.*

During this period, record low stratospheric temperature in the satellite era were just equatorward of the polar vortex edge (Figure 4.5b). These months are also when stratospheric planetary activity becomes important to the circulation variability. Hunga may impact stratospheric circulation not only through radiative forcing but also by modifying wave–mean flow interactions.

Temperature anomalies with horizontal gradients imply the existence of vertical wind shear anomalies through thermal wind balance. In austral winter 2022, the maximum stratospheric cooling was consistent with positive and negative vertical wind shears equatorward and poleward, respectively, leading to positive wind anomalies of over 40 m s^{-1} at 40°S in the upper stratosphere shown in MERRA-2 (Figure 4.7). The location of the large wind anomaly amplitudes coin-

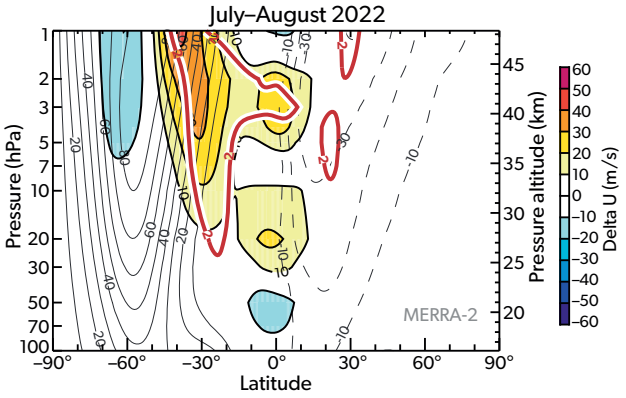

Figure 4.7: *Zonal mean zonal wind anomaly for July and August 2022. The grey contours show the background zonal winds with an interval of 10 m s^{-1}. MERRA-2 wind anomalies are calculated relative to the 2005-2021 mean and 2005-2023 trend. Red contours highlight anomalies exceeding 2 standard deviations.*

cided with the location of the polar vortex at these altitudes. The enhanced zonal winds in this region exceeded the range of internal variability observed in previous years (Wang et al., 2023). The other three reanalyses produce a similar pattern and magnitude (not shown).

In addition, we investigated the evolution of the global averaged temperature anomalies using the Reanalysis Intercomparison Dataset (Martineau et al., 2018) for the four reanalyses. Global temperature anomalies for the years 2022 to 2024 are shown in Figure 4.8. The anomalies were obtained by regressing out the components of the seasonal cycle, linear trend, the QBO, solar cycle, and ENSO (Niño 3.4) for the period 1980–2023, excluding the 24 months after the three major tropical eruptions (from January 2022 to December 2023 for the Hunga eruption). In MERRA-2, negative temperature anomalies first appeared around 20 hPa in April 2022, ascending to around 5 hPa by one year later. Separately, there is a continuous negative temperature anomaly around 1 hPa throughout the year 2022. These features are similar to the MLS measurements shown in Figure 4.3, in part because MLS temperature retrievals have been assimilated in this reanalysis.

Other reanalyses JRA-3Q, ERA5, and JRA-55 show generally similar negative anomalies of -0.5 K in the mid-stratosphere around 20–10 hPa, but do not show ascending anomalies up to 5 hPa. This is probably because these latter three reanalyses do not assimilate MLS temperatures, and other temperature-sensitive microwave and infrared satellite sounders may not be able to strongly constrain upper stratospheric temperatures in these reanalysis systems. Also, the negative anomalies are much weaker in JRA-3Q than in the other three reanalyses; this is in part because in JRA-3Q, mid-stratospheric subtropical positive anomalies are much greater, partially cancelling the SH mid latitude negative anomalies in the global means.

Overall, global DA systems tracked the observed cooling anomalies up to the mid-stratosphere despite the modelling component being unaware of the composition perturbation following the Hunga eruption. Above about the 10 hPa level, MERRA-2 is the only reanalysis that provides similar temperature signals to those in the MLS observations because MERRA-2 is the only reanalysis that assimilates MLS temperature retrievals above the 5 hPa level. In addition, these reanalyses provide global information on winds and circulation patterns, with multi-year reanalysis products enabling potential identification of post-Hunga eruption anomalies.

4.2.3 Hunga induced temperature and circulation anomalies in models

Global atmospheric models can isolate the effects of the Hunga eruption on temperatures and winds through the use of control and ensemble simulations, aiding in our understanding of these impacts. Using multiple ensemble members with slightly perturbed initial conditions can capture natural variability while the volcanic perturbations to atmospheric composition can be excluded in control runs or included in volcano runs. The forced signal induced by Hunga can be extracted by the statistically significant differences between the volcano and the control ensembles.

Here, we analyse four models that participated in the Hunga Tonga-Hunga Ha'apai Volcano Impact Model Observation Comparison (HTHH-MOC) Project (Zhuo et al., 2025): Community Earth System Model, version 2 / Whole Atmosphere Community Climate Model version 6 (CESM2/WACCM6, hereafter referred to as WACCM) with modal aerosol module (MAM), Goddard Earth Observing System earth system model (GEOSCCM), Goddard Space Flight Center two-dimensional model (GSFC2D), and the Model for Interdisciplinary Research on Climate – Chemical Atmospheric general circulation model for Study of atmospheric Environment and Radiative forcing (MIROC-CHASER). After adding realistic amounts of H_2O and SO_2 perturbations from the Hunga eruption in January 2022, all models can capture the evolution of the water vapour and temperature perturbations on a global scale (see detailed com-

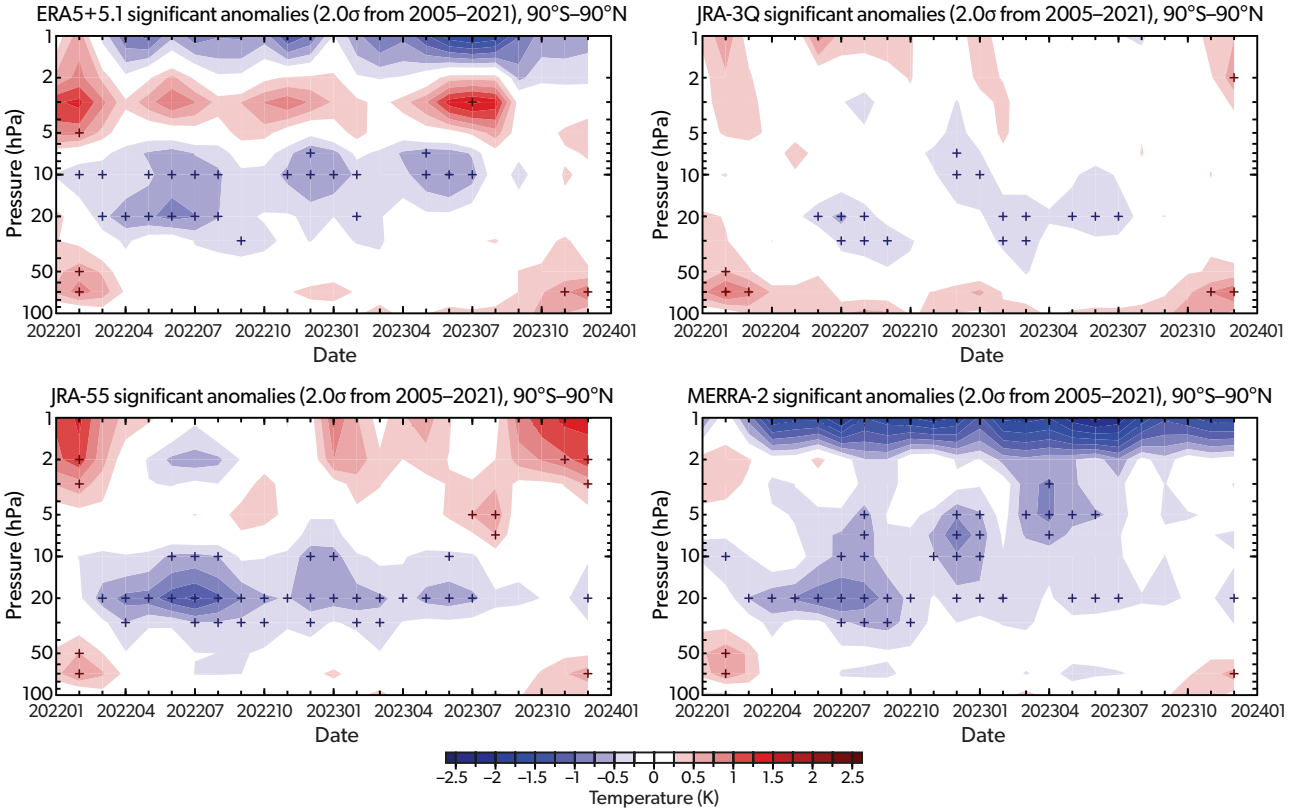

Figure 4.8: *Global-mean temperature anomalies in the stratosphere from the ERA5, JRA-3Q, JRA-55, and MERRA-2 reanalyses. These anomalies were obtained by regressing out the components of seasonal cycle, linear trend, the QBO, solar cycle, and ENSO for the period 1980-2023, excluding the 24 months after the three major tropical eruptions, for each reanalysis. The hatched regions are those evaluated as significant based on twice of the standard deviation of the anomalies for the period 2005-2021. Note that MERRA-2 assimilated temperature retrievals from Aura MLS at pressures 5 hPa and less, but the other three did not.*

parison and Figure 4 in Zhuo et al., 2025). The global time-height temperature response from WACCM is shown in Figure 4.9 as a reference. Notable similarities to the observations (Figure 4.3) include the ascent of the cooling of ~0.5 K overlapping the H_2O cloud, followed by a systematically larger temperature response in the mesosphere. Note that global average data show very small warming effects from Hunga aerosol in the lower stratosphere in both observations and model simulations, so the main Hunga impacts on temperature appear to be due to the radiative cooling effects of H_2O.

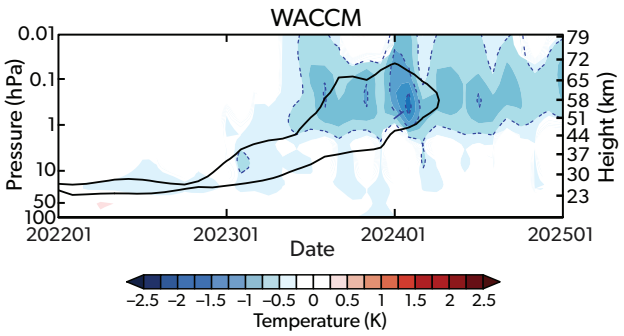

Figure 4.9: *Modelled global mean temperature perturbation (color shading at 0.5 K intervals) as a function of pressure and time from CESM2-WACCM6. Solid black contour shows the location of forecasted H_2O plume at 1 ppmv level. Regions where differences are not significant at the 95% level using t-test are shaded white.*

During austral winter months in 2022, the WACCM ensemble mean averaged over 60 ensemble members reproduced the strong monthly mean negative temperature anomaly in the SH (Figure 4.10a), matching the altitudes and latitudes in the observations (Figure 4.5b), but with a weaker magnitude. The simulated zonal wind changes also show a strengthening and equatorward displacement of the winter westerlies in response to the Hunga forcing (Figure 4.10b), with patterns similar to the observed anomalies (Figure 4.7). Both the ensemble mean temperature and mean wind anomalies in the model ensemble are only about half as pronounced as those observed in 2022. Despite the smaller magnitude, the similarity in timing and

spatial structure of observed and modelled temperature and wind patterns is strongly suggestive of an Hunga attribution for the observed anomalies. GEOSCCM with 10 ensemble members did show a cooling signal in this region during the same months, but it was not statistically significant at 95% level (Figure 4.10c). The GSFC2D model (Figure 4.10d) uses specified lower tropospheric forcing for the planetary and gravity wave parameterisations that is identical for both the control and Hunga runs, thus lacking possible wave–mean flow feedbacks due to the Hunga eruption. The internal variability is very small in the 2D model, and it captures only small dynamical changes due to the direct radiative impacts of the Hunga H_2O and aerosol. It simulates significant cooling of about 2 to 3 K in the tropical stratosphere near 20 hPa, with weaker warming below the cooling layer. The 2D model does not reproduce the mid latitude cooling in the ensemble mean, which is consistent with the hypothesis that the observed mid latitude cooling anomalies in austral winter 2022 are a combination of the dynamical (wave) response to Hunga's radiative forcing and internal (unforced) variability. The MIROC-CHASER model simulates cooling in regions overlapping the Hunga H_2O, but it does not reproduce the mid latitude cooling and underestimates sulfate concentrations and the associated infrared heating (Figure 4.10e).

These discrepancies among the models and observations suggest that while the radiative effect of H_2O is a robust feature of the Hunga eruption's impact, not all global climate models reproduce the strong mid latitude cooling pattern with statistical significance, indicating that the observed response may contain significant internal variability (Yu et al., 2023).

Reasons behind the specific patterns of temperature and wind observed in 2022, and how those patterns are related to the Hunga water and aerosol anomalies, continue to be an active research topic (Yook et al., 2025). Ongoing research should provide additional insights into the dynamical processes, that is, the relationships between the temperature, wind, and wave anomalies, in these observed fields.

As the water vapour anomaly spread into the NH it was blocked by the formation of the NH stratospheric jet (Figure 4.1b), and did not reach the coldest regions of NH 2022/2023 winter stratospheric polar vortex (Chapter 3). However, the possibility of anomalous cooling outside of the vortex and at upper levels, modifying the evolution of the NH polar region, remains to be fully explored (Kuchar et al., 2025). Reanalysis shows that zonal mean zonal winds during the 2022/2023 winter were within the range of internal variability (supplementary Figure S4.1), and the MLS temperatures show no clear or persistent departures from the mean state (supplementary Figure S4.2). Current modelling research suggests Hunga effects at a level much smaller than annual variability (Figure S3.28), and therefore it is difficult to identify or quantify any Hunga signal (Bednarz et al., 2026). These results highlight the need for additional studies using larger model ensemble sizes to constrain the role of the Hunga eruption in modulating the NH stratospheric circulation (Figure S3.33).

4.3 Residual mean meridional circulation and Eliassen-Palm flux

Comparisons between global DA systems and models can provide complete diagnostics on the effects of the Hunga eruption on the atmospheric circulation. Here, the focus is on the effects of the Hunga eruption on the mean meridional transport circulation (residual mean circulation RMC) and its wave forcing as diagnosed by the Eliassen-Palm flux (EP flux).

4.3.1 Residual mean meridional circulation and EP flux in the global data assimilation systems

In the austral winter months following the Hunga eruption, the RMC developed a clockwise anomaly, which indicates anomalous SH mid-latitude upwelling and low-latitude downwelling that opposes and weakens the normal background circulation (Figure 4.11a). By austral winter of 2022, this RMC anomaly encompassed the vertical extent of the SH stratosphere and extended into the NH in the lower stratosphere in MERRA-2 (Figure 4.11a). It is important to note that the full RMC remained downward in the SH high latitudes. However, it was weakened by the anomaly. These circulation anomalies remained as strong clockwise circulation anomalies during June to August 2022, based on the 43-year (1980–2022) MERRA-2 dataset (Coy et al., 2022). Note that the "upward" residual circulation anomaly in the SH extratropics is consistent with the cold anomaly (Figure 4.6), as the RMC anomaly reduced the adiabatic heating from the climatological downward RMC. The downward anomaly in the tropics, however, would be associated with anomalous warming, which would oppose the radiative signal.

The wave forcing of the stratosphere also displayed significant changes after the Hunga eruption. EP

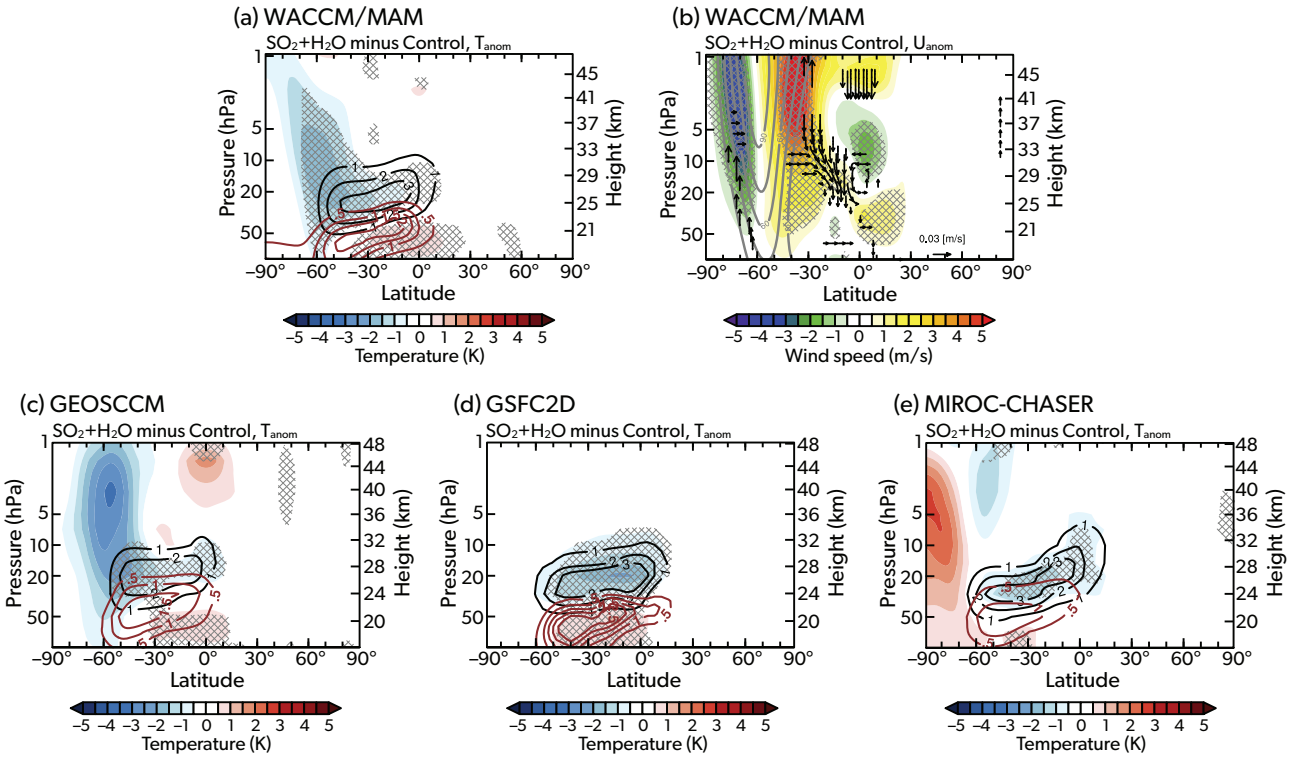

Figure 4.10: *Modelled temperature differences in July and August 2022 (colour shading, K) from (a) WACCM with modal aerosol module (MAM), (c) GEOSCCM, (d) GSFC2D, and (e) MIROC-CHASER. Red contours denote the sulfate aerosol extinction at 745 nm in 10^{-3} km^{-1}, and black contours denote the anomalous H_2O concentration in ppmv. (b) Zonal mean zonal wind differences averaged in July and August 2022. Colours show zonal mean zonal wind anomalies in WACCM simulations compared to the control runs. Gray contours show the background zonal winds with an interval of 15 m s^{-1}. The vectors depict the significant anomalies in the residual mean circulation. Hatched regions indicate where anomalies are statistically significant at the 95% level according to Student's* t*–test.*

fluxes are a measure of the propagation of wave activity. In the SH winter climatology, EP fluxes are upward and equatorward, as these waves are typically forced from the troposphere. Along with the zonal wind, temperature, and RMC anomalies, the July–August 2022 upward and equatorward EP fluxes were reduced in high latitudes at 60°S throughout the stratosphere (Figure 4.11b). Since the climatological EP fluxes are upward, the downward EP flux anomalies in Figure 4.11b indicate weaker upward EP flux from the mid-stratosphere upward over 40°S–60°S and hence, reduced planetary wave activity in austral winter 2022. Note that there was some increase in the upward and equatorward EP flux vectors in the lower to mid stratosphere near 45°S. Since the planetary waves preferably propagate in the regions of strong potential vorticity gradients, this equatorward shift in EP flux was consistent with a more equatorward expanded polar vortex in 2022 (Wang et al., 2023).

With reduced upward EP fluxes, the wave forcing of the zonal mean zonal flow from the flux divergence results in reduced drag, leading to strengthening of the polar vortex. Climatologically, wave activity acts to decelerate the zonal mean zonal wind in the region of the polar vortex, i.e., EP flux divergence is negative. The July–August 2022 EP flux divergence anomaly is accelerating the zonal mean zonal wind in the SH upper stratosphere (Figure 4.10b), and thus acting to reduce the climatological drag on the zonal wind.

4.3.2 Residual mean circulation and EP flux changes in models

Detailed comparisons of simulated anomalies from global models against DA results confirm the models' ability to simulate the RMC and EP fluxes. The WACCM simulation, used as an example, has been able to represent the RMC anomalies in austral winter months during 2022. The upward residual circulation anomaly at 60°S and downward anomaly extending across the equator (Figure 4.10b) compares well with the DA-derived RMC in Figure 4.11a. The changes in the RMC are associated with adiabatic cooling in the stratosphere in the SH extratropics, consistent with a weakened planetary-scale wave forcing in the middle

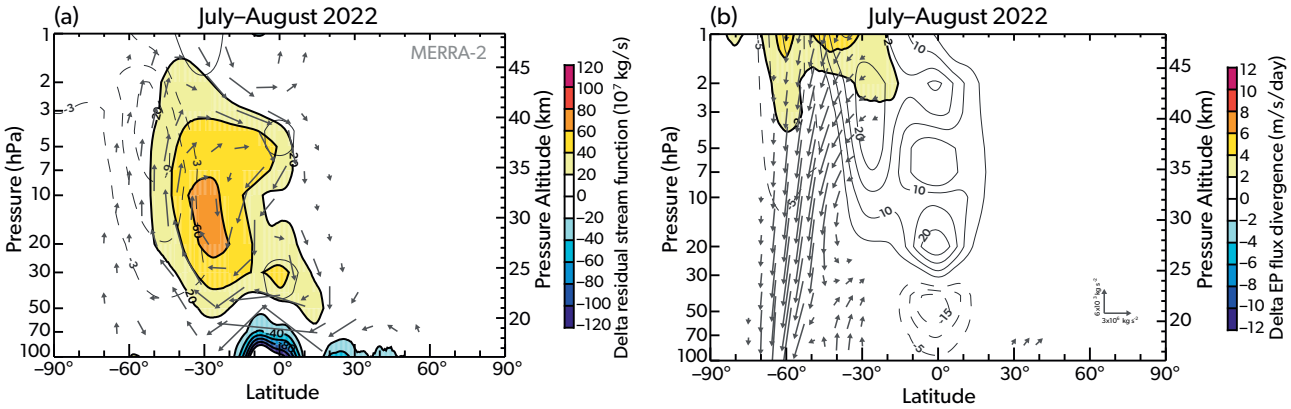

Figure 4.11: *(a) Monthly mean residual circulation anomaly for July-August 2022. The arrows show the circulation calculated from the stream function anomaly. The dashed contours show the corresponding temperature anomaly (K) for the same month. (b) EP flux divergence anomalies for July-August 2022 (filled contours) and EP flux anomaly vectors (arrows). The scale arrows are 3x10^6 kg s^{-2} for the meridional component and 6x10^3 kg s^{-2} for the vertical component. The grey contours show the corresponding zonal mean zonal wind anomaly (m s^{-1}). Fields are shown relative to the 2005-2021 mean, with the 2005-2023 linear trend subtracted.*

and upper stratosphere.

The coupling of planetary wave amplitudes and stratospheric temperature is a well-known feature of the winter stratosphere (Andrews et al., 2016; Randel and Newman, 1998). The correlation is evident in Figure 4.12, which shows results from all available WACCM ensemble members in the HTHH-MOC Project (Zhuo et al., 2025), consisting of 60 Hunga-forced and 60 control simulations. Over July and August from 2022 to 2031, a significant positive correlation (r = 0.76, p-value < 0.0001) is found between polar temperature versus the vertical component of the EP flux in the lower stratosphere (grey dots). Among the 60 Hunga-forced ensemble members, 44 runs exhibit a cold temperature anomaly in 2022 (red dots in Figure 4.12), and several simulations produce temperature and wave responses comparable to the observations (black dot in Figure 4.12). There is a systematic shift in temperatures and wave activity in the integrations with the eruption in 2022 (red dots in Figure 4.12) with respect to the 10-year control ensemble background (grey dots in Figure 4.12). Specifically, 39 out of 60 ensemble members (65%) exhibit both colder temperatures and weaker upward EP fluxes in response to the Hunga eruption, compared to 42% in the control ensemble. We view this shift as a fingerprint of the response to the Hunga forcing in WACCM simulations. However, there is considerable stochastic variability among the volcano realisations. We conclude that internal variability in the ensemble model simulations contributes to the weaker amplitudes of the ensemble average temperature and wind anomalies compared to the observed pattern in 2022. Similar strong correlations between temperature and wave activities are found in the other two 3D models (supplementary Figure S4.3). However, the Hunga-forced simulations in these models exhibit considerable spread, and with only 10 ensemble members, it is difficult to determine whether there is a clear shift toward colder temperatures.

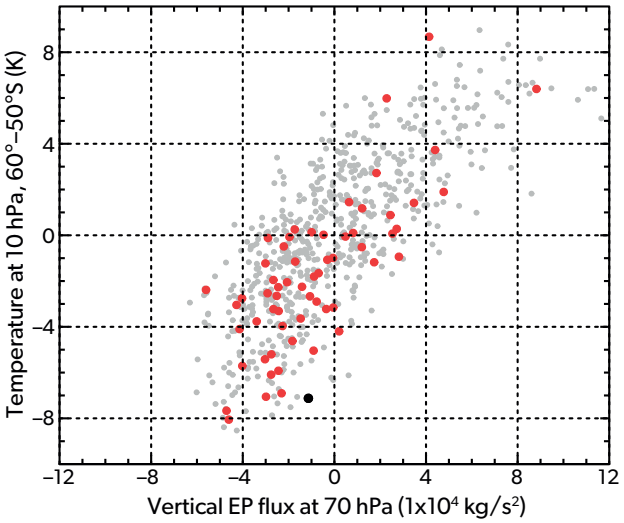

Figure 4.12: *Relationship between July–August average temperatures at 10 hPa and upward EP flux at 70 hPa over 55°S–65°S. Red dots represent the Hunga-forced minus control WACCM simulation for July–August 2022, based on 60 ensemble members. Gray dots represent deviations from the control ensemble mean for July–August averages across 2022–2031 (60 ensemble members over 10 years). The black dot indicates the July–August 2022 average from ERA5.*

4.4 Interaction of Hunga with the Quasi-Biennial Oscillation (QBO)

The Quasi-Biennial Oscillation (QBO) occurs in the lower stratosphere near the equator, manifesting as alternating easterlies and westerlies that descend from the stratopause to the tropopause with a period of ~28 months (Baldwin et al., 2001). Such equatorial zonal wind anomalies are balanced by a meridional circulation that extends temperature anomalies throughout the tropical stratosphere (Plumb and Bell, 1982). Depending on the QBO phase, the QBO meridional circulation may reinforce or weaken the background RMC.

In early 2022, QBO had easterly winds in the lower stratosphere with westerly winds above (Figure 4.13), a configuration associated with a lower stratosphere secondary circulation descending at the equator and ascending at the subtropics. Such a circulation may have enhanced the cross-equatorial transport of water vapour following the Hunga eruption (Schoeberl et al., 2023). Jucker et al. (2024) further suggested from their chemistry-climate model simulations that excessive stratospheric water vapour like that injected by the Hunga eruption tends to stay longer in the middle atmosphere if the QBO is in the easterly phase than the westerly phase at 50 hPa, as observed in 2022, and effects of the initial easterly QBO phase could persist over a few years (Diallo et al., 2018; Jucker et al., 2024).

Given the potential impact of the QBO on RMC, austral winter 2022 offers an opportunity for comparing the QBO-induced circulation anomaly to the changes caused by the Hunga eruption. The QBO signal in RMC is derived from the 1980-2021 MERRA-2 record by averaging daily July–August residual mean circulations on days with a similar QBO phase to July–August 2022. The estimated QBO effect on the RMC (Figure 4.14a) generally opposed the August 2022 residual circulation in the SH (Figure 4.11b), resulting in a slight reduction in the strength of the austral winter 2022 residual circulation anomaly (Figure 4.14b), especially equatorward of 30°S latitude. The QBO-induced residual circulation anomaly in the upper stratosphere (above the main QBO region) shows a downward circulation just equatorward of the main cold anomaly, which may have had a minor influence in limiting the equatorward extent of the cold anomaly. However, since the QBO signal in residual circulation is much weaker than the full residual circulation, and does not extend into the main cooling anomaly region (40°–60°S) during July–August 2022,

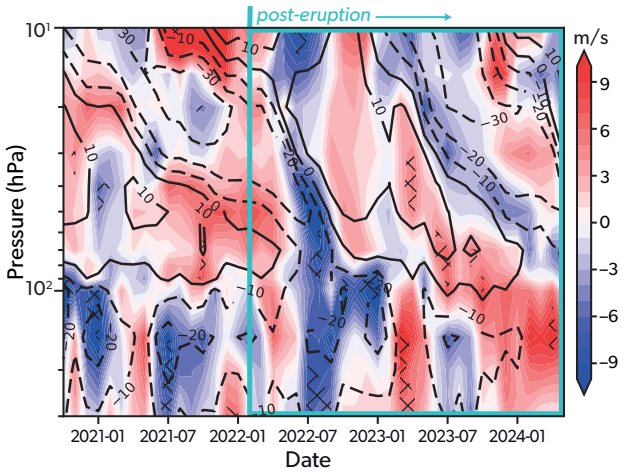

Figure 4.13: *Monthly mean zonal wind measured by radiosondes from the Meteorological Service Singapore Upper Air Observatory (station code 48698) (black contours) and its differences with respect to the months between 1979-2014 that has similar QBO phase (colour shading, unit: m/s). QBO phase is determined by the two leading EOFs in the Singapore wind between 100-10 hPa following Wallace et al. (1993). We compare the wind profile in each month to those months that have QBO phase within ±0.1π of this month, representing a small fraction of the QBO cycle. Hatches indicate the differences that are statistically significant at 90% confidence level based on the Student's t-test. The turquoise box marks the period after the eruption. The turquoise box marks the common region plotted in Figure 4.15.*

it does not appear to have played a major role in the creation and maintenance of the cold anomaly. Therefore, this suggests that the anomalous temperature and RMC responses in the mid-latitude were primarily caused by the large internal variability and the Hunga forcing.

The QBO progression before and after the Hunga eruption in radiosonde observations shows that the equatorial zonal wind was easterly between 20 hPa and 60 hPa in early 2022 when the Hunga volcano erupted (Figure 4.13). These easterlies descended over the next few months, and westerlies dominated the equatorial stratosphere in late 2022. By early 2024, the wind profile returned to a similar structure as in early 2022, corresponding to a period of ~2 years. This particular QBO cycle is faster than the average period (~28 months) but is still within the range of variations seen in observations over the past few decades.

The amplitude of the QBO following the eruption showed some significant regions of stronger than usual westerlies and easterlies (Figure 4.13). However, the easterly anomalies are significant only for one month below 60 hPa in 2022, and the westerlies

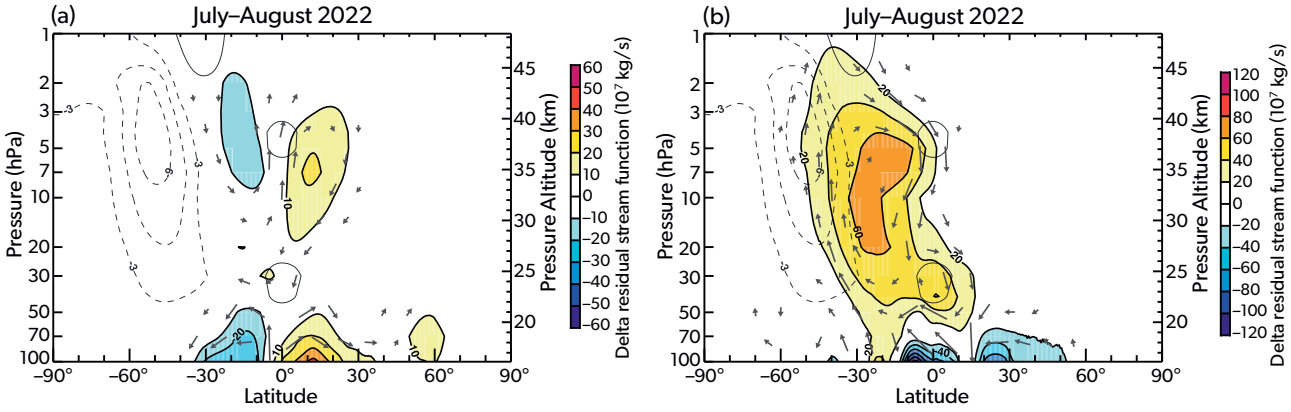

Figure 4.14: *(a) Estimated QBO signal in the residual mean circulation, calculated as the average circulation during July-August of years with similar QBO phase as in 2022; (b) Residual mean circulation after QBO-induced circulation shown in (a) from the full circulation shown in Figure 4.11a. Gray contours denote the July-August 2022 temperature anomaly. The arrow lengths, based on the stream function, are scaled by pressure. Note that the contour interval is halved in (a) relative to (b) and that the scale of the arrows in (a) are double the arrow scale in (b). All fields are from MERRA-2.*

appear for just three months in the lower stratosphere. It is difficult to attribute these changes to the Hunga eruption given the complicated interaction between the waves generated from convection in the troposphere and the stratospheric circulation responsible for creating the highly variable QBO.

We also examined the QBO simulated across all models participating in HTHH-MOC, enabling the examination of equatorial zonal wind anomalies due to the additional sulfate aerosols and water vapour from the eruption (Figure 4.15). The models did not simulate a statistically significant response to the Hunga eruption in the equatorial winds over most of the stratosphere and mesosphere. Instead, they revealed a generally insignificant weakening of QBO amplitude from 2023 onward, a result that disagrees with the stronger anomalies observed. Models are known to have problems simulating the QBO, including producing a wind oscillation that is too weak in the lower stratosphere, not capturing the ozone feedback, and not having the correct gravity wave spectrum (Anstey et al., 2022). The possible inability of models to simulate a realistic QBO limits our ability to say whether the QBO changes in observations are part of natural variability or a result of the forced response to the eruption.

4.5 Summary

Satellite and reanalysis systems demonstrated persistent perturbations in stratospheric temperature and circulation following the Hunga eruption. The Hunga H_2O injected by the eruption in 2022 remains until the present in 2025. It was spread globally by the Brewer-Dobson circulation, which includes vertical and meridional transport by the residual mean circulation and mixing along isentropic surfaces.

During the austral winter months in 2022, observations showed large-scale SH stratospheric cooling, consistent with the equatorward shift of the SH winter stratospheric jet and the slowing of the residual mean circulation with reduced wave activity seen in the DA system. In the first two years following the Hunga volcanic eruption, the global average stratospheric temperatures decreased by 0.5 to 1.0 K. This impact was mainly due to radiative cooling from H_2O injected into the stratosphere by the Hunga eruption. The observed cooling patterns rose in altitude over time following the evolution of the H_2O plume. Unlike earlier sulfur-rich volcanoes, satellite observations provide little evidence of global warming impacts from Hunga aerosols in the lower stratosphere.

Global atmospheric models were used to isolate the effects of the Hunga eruption on stratospheric temperatures and winds by distinguishing volcanic forcing from natural variability. Simulations from the HTHH-MOC Project, including WACCM, GEOSCCM, GSFC2D, and MIROC-CHASER, tracked the evolution of water vapour and temperature perturbations, showing ~0.5 K global stratospheric cooling overlapping the H_2O cloud and a stronger response in the mesosphere. While all models captured the radiative cooling due to Hunga H_2O, not all global chemistry-climate models reproduced the large-scale Southern Hemisphere cooling and equatorward-shifted polar vortex. This suggests that the observed mid latitude temperature anomalies might contain substantial

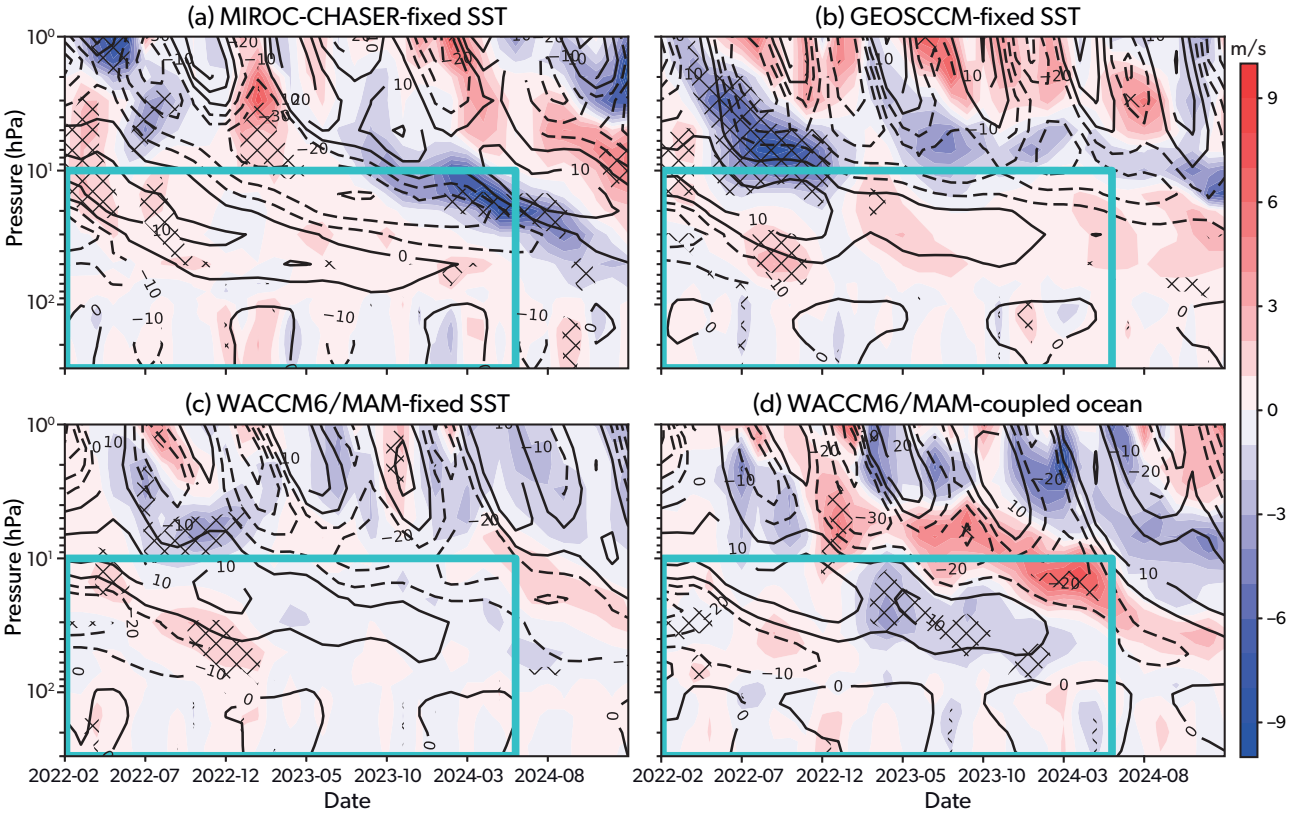

Figure 4.15: *Ensemble mean equatorial zonal mean zonal wind averaged over 5°N-5°S simulated in (a) MIROC-CHASER fixed SST runs (b) GEOSCCM fixed SST runs (c) WACCM fixed SST runs and (d) WACCM coupled ocean runs. Black contours represent the equatorial winds in no-volcano runs, while colour shading shows anomalies due to volcanic aerosols and water vapour in units of m s^{-1}. Diagonal hatches indicate differences between the two simulations are statistically significant at 90% confidence level. Statistical significance is estimated based on the two-sided Student's t–test. The turquoise box marks the common region plotted in Figure 4.13.*

internal variability, with local Hunga impacts intertwined with dynamically forced anomalies.

While a slightly faster and stronger QBO was observed following the Hunga eruption, this change was within the range of variability and was not simulated across the participating models in the HTHH-MOC activity, indicating that the eruption likely had no significant impact on the QBO.

References

Andrews, D. G., C. B. Leovy and J. R. Holton (2016). *Middle Atmosphere Dynamics*. Vol. 40. Academic Press.

Anstey, J. A., S. M. Osprey, J. Alexander, M. P. Baldwin, N. Butchart, L. Gray, Y. Kawatani, P. A. Newman and J. H. Richter (2022). 'Impacts, processes and projections of the quasi-biennial oscillation'. *Nature Rev. Earth Environ.*, 3, pp. 588–603. DOI: 10.1038/s43017-022-00323-7.

Baldwin, M. P., L. J. Gray, T. J. Dunkerton, K. Hamilton, P. H. Haynes, W. J. Randel, J. Holton, M. J. Alexander, I. Hirota and T. Horinouchi (2001). 'The quasi-biennial oscillation'. *Rev. Geophys.*, 39, pp. 179–229. DOI: 10.1029/1999rg000073.

Bednarz, E. M., A. H. Butler, X. Wang, Z. Zhuo, W. Yu, G. Stenchikov, M. Toohey and Y. Zhu (2026). 'Indirect climate impacts of the Hunga eruption'. *Atmos. Chem. Phys.*, 26, pp. 197–215. DOI: 10.5194/acp-26-197-2026.

Carn, S. A., N. A. Krotkov, B. L. Fisher and C. Li (2022). 'Out of the blue: volcanic SO_2 emissions during the 2021-2022 Hunga Tonga-Hunga Ha'apai eruptions'. *Front. Earth Sci.*, 13. DOI: 10.3389/feart.2022.976962.

Coy, L., P. Newman, K. Wargan, G. Partyka, S. Strahan and S. Pawson (2022). 'Stratospheric Circulation Changes Associated with the Hunga Tonga-Hunga Ha'apai Eruption'. *Geophys. Res. Lett.*, 49, e2022GL100982. DOI: 10.1029/2022GL100982.

Diallo, M., M. Riese, T. Birner, P. Konopka, R. Müller, M. I. Hegglin, M. L. Santee, M. Baldwin, B. Legras and F. Ploeger (2018). 'Response of stratospheric water vapor and ozone to the unusual timing of El Niño and the QBO disruption in 2015–2016'. *Atmos. Chem. Phys.*, 18, pp. 13055–13073. DOI: 10.5194/acp-18-13055-2018.

Duchamp, C., F. Wrana, B. Legras, P. Sellitto, R. Belhadji and C. von Savigny (2023). 'Observation of the aerosol plume from the 2022 Hunga Tonga–Hunga Ha'apai eruption with SAGE III/ISS'. *Geophys. Res. Lett.*, 50, e2023GL105076. DOI: 10.1029/2023GL105076.

Gelaro, R., W. McCarty, M. J. Suárez, R. Todling, A. Molod, L. Takacs, C. A. Randles, A. Darmenov, M. G. Bosilovich and R. Reichle (2017). 'The Modern-Era Retrospective Analysis for Research and Applications, Version 2 (MERRA-2)'. *J. Climate*, 30, pp. 5419–5454. DOI: 10.1175/jcli-d-16-0758.1.

Gupta, A. K., T. Mittal, K. E. Fauria, R. Bennartz and J. F. Kok (2025). 'The January 2022 Hunga eruption cooled the Southern Hemisphere in 2022 and 2023'. *Commun. Earth Environ.*, 6, 240. DOI: 10.1038/s43247-025-02181-9.

Hersbach, H., B. Bell, P. Berrisford, S. Hirahara, A. Horányi, J. Muñoz-Sabater, J. Nicolas, C. Peubey, R. Radu, D. Schepers et al. (2020). 'The ERA5 global reanalysis'. *Q. J. R. Meteorol. Soc.*, 146, pp. 1999–2049. DOI: 10.1002/qj.3803.

Hitchcock, P., T. G. Shepherd and S. Yoden (2010). 'On the approximation of local and linear radiative damping in the middle atmosphere'. *J. Atmos. Sci.*, 67, pp. 2070–2085. DOI: 10.1175/2009jas3286.1.

Jucker, M., C. Lucas and D. Dutta (2024). 'Long-term climate impacts of large stratospheric water vapor perturbations'. *J. Climate*, 37, pp. 4507–4521. DOI: 10.1175/JCLI-D-23-0437.1.

Khaykin, S., A. Podglajen, F. Ploeger, J.-U. Grooß, F. Tence, S. Bekki, K. Khlopenkov, K. Bedka, L. Rieger, A. Baron et al. (2022). 'Global perturbation of stratospheric water and aerosol burden by Hunga eruption'. *Commun. Earth Environ.*, 3, 316. DOI: 10.1038/s43247-022-00652-x.

Kobayashi, S., Y. Ota, Y. Harada, A. Ebita, M. Moriya, H. Onoda, K. Onogi, H. Kamahori, C. Kobayashi and H. Endo (2015). 'The JRA-55 reanalysis: General specifications and basic characteristics'. *J. Meteorol. Soc. Japan. Ser. II*, 93, pp. 5–48. DOI: 10.2151/jmsj.2015-001.

Kosaka, Y., S. Kobayashi, Y. Harada, C. Kobayashi, H. Naoe, K. Yoshimoto, M. Harada, N. Goto, J. Chiba and K. Miyaoka (2024). 'The JRA-3Q reanalysis'. *J. Meteorol. Soc. Japan. Ser. II*, 102, pp. 49–109. DOI: 10.2151/jmsj.2024-004.

Kuchar, A., T. Sukhodolov, G. Chiodo, A. Jörimann, J. Kult-Herdin, E. Rozanov and H. H. Rieder (2025). 'Modulation of the northern polar vortex by the Hunga Tonga–Hunga Ha'apai eruption and the associated surface response'. *Atmos. Chem. Phys.*, 25, pp. 3623–3634. DOI: 10.5194/acp-25-3623-2025.

Labitzke, K. and M. P. McCormick (1992). 'Stratospheric temperature increases due to Pinatubo aerosols'. *Geophys. Res. Lett.*, 19, pp. 207–210. DOI: 10.1029/91gl02940.

Legras, B., C. Duchamp, P. Sellitto, A. Podglajen, E. Carboni, R. Siddans, J.-U. Grooß, S. Khaykin and F. Ploeger (2022). 'The evolution and dynamics of the Hunga Tonga–Hunga Ha'apai sulfate aerosol plume in the stratosphere'. *Atmos. Chem. Phys.*, 22, pp. 14957–14970. DOI: 10.5194/acp-22-14957-2022.

Martineau, P., J. S. Wright, N. Zhu and M. Fujiwara (2018). 'Zonal-mean data set of global atmospheric reanalyses on pressure levels'. *Earth Syst. Sci. Data*, 10, pp. 1925–1941. DOI: 10.5194/essd-10-1925-2018.

Millán, L., W. G. Read, M. L. Santee, A. Lambert, G. L. Manney, J. L. Neu, M. C. Pitts, F. Werner, N. J. Livesey and M. J. Schwartz (2024). 'The Evolution of the Hunga Hydration in a Moistening Stratosphere'. *Geophys. Res. Lett.*, 51, e2024GL110841. DOI: 10.1029/2024gl110841.

Millán, L., M. L. Santee, A. Lambert, N. J. Livesey, F. Werner, M. J. Schwartz, H. C. Pumphrey, G. L. Manney, Y. Wang, H. Su et al. (2022). 'The Hunga Tonga-Hunga Ha'apai Hydration of the Stratosphere'. *Geophys. Res. Lett.*, 49, e2022GL099381. DOI: 10.1029/2022gl099381.

Plumb, R. A. and R. C. Bell (1982). 'A model of the quasi-biennial oscillation on an equatorial beta-plane'. *Q. J. R. Meteorol. Soc.*, 108, pp. 335–352. DOI: 10.1002/qj.49710845604.

Plumb, R. A. (1996). 'A "tropical pipe" model of stratospheric transport'. *J. Geophys. Res.*, 101, pp. 3957–3972. DOI: 10.1029/95JD03002.

Randel, W. J. and P. A. Newman (1998). 'The stratosphere in the Southern Hemisphere'. *Meteorol. South. Hemisphere*. Springer, pp. 243–282. DOI: 10.1007/978-1-935704-10-2_9.

Randel, W. J., X. Wang, J. Starr, R. R. Garcia and D. Kinnison (2024). 'Long-Term Temperature Impacts of the Hunga Volcanic Eruption in the Stratosphere and Above'. *Geophys. Res. Lett.*, 51. DOI: 10.1029/2024gl111500.

Rieger, L. A., W. J. Randel, A. E. Bourassa and S. Solomon (2021). 'Stratospheric temperature and ozone anomalies associated with the 2020 Australian New Year fires'. *Geophys. Res. Lett.*, 48, e2021GL095898. DOI: 10.1029/2021gl095898.

Schoeberl, M. R., Y. Wang, R. Ueyama, G. Taha and W. Yu (2023). 'The Cross Equatorial Transport of the Hunga Tonga-Hunga Ha'apai Eruption Plume'. *Geophys. Res. Lett.*, 50, e2022GL102443. DOI: 10.1029/2022gl102443.

Sellitto, P., A. Podglajen, R. Belhadji, M. Boichu, E. Carboni, J. Cuesta, C. Duchamp, C. Kloss, R. Siddans, N. Bègue et al. (2022). 'The unexpected radiative impact of the Hunga Tonga eruption of 15th January 2022'. *Commun. Earth Environ.*, 3, 288. DOI: 10.1038/s43247-022-00618-z.

Simmons, A., C. Soci, J. Nicolas, B. Bell, P. Berrisford, R. Dragani, J. Flemming, L. Haimberger, S. Healy, H. Hersbach et al. (2020). 'Global stratospheric temperature bias and other stratospheric aspects of ERA5 and ERA5.1'. *ECMWF Technical Memoranda*, DOI: 10.21957/rcxqfmg0.

SPARC (2022). *Reanalysis Intercomparison Project (S-RIP) Final Report*. Tech. rep. SPARC Report No. 10, WCRP-6/2021. https://www.aparc-climate.org/sparc-reports/sparc-report-no-10/. SPARC/WCRP.

Steiner, A. K., F. Ladstädter, W. J. Randel, A. C. Maycock, Q. Fu, C. Claud, H. Gleisner, L. Haimberger, S.-P. Ho and P. Keckhut (2020). 'Observed temperature changes in the troposphere and stratosphere from 1979 to 2018'. *J. Climate*, 33, pp. 8165–8194. DOI: 10.1175/jcli-d-19-0998.1.

Vömel, H., S. Evan and M. Tully (2022). 'Water vapor injection into the Stratosphere by Hunga Tonga-Hunga Ha'apai'. *Science*, 377, pp. 1444–1447. DOI: 10.1126/science.abq2299.

Wallace, J. M., R. L. Panetta and J. Estberg (1993). 'Representation of the Equatorial Stratospheric Quasi-Biennial Oscillation in EOF Phase Space'. *J. Atmos. Sci.*, 50, pp. 1751–1762. DOI: 10.1175/1520-0469(1993)050<1751:ROTESQ>2.0.CO;2.

Wang, X., W. Randel, Y. Zhu, S. Tilmes, J. Starr, W. Yu, R. Garcia, O. B. Toon, M. Park, D. Kinnison et al. (2023). 'Stratospheric Climate Anomalies and Ozone Loss Caused by the Hunga Tonga-Hunga Ha'apai Volcanic Eruption'. *J. Geophys. Res.*, 128, e2023JD039480. DOI: 10.1029/2023jd039480.

Wang, Y. and Y. Huang (2024). 'Compensating atmospheric adjustments reduce the volcanic forcing from Hunga stratospheric water vapor enhancement'. *Sci. Adv.*, 10, eadl2842. DOI: 10.1126/sciadv.adl2842.

Yook, S., S. Solomon and X. Wang (2025). 'The impact of 2022 Hunga Tonga-Hunga Ha'apai (Hunga) eruption on stratospheric circulation and climate'. *J. Geophys. Res.*, 130, e2024JD042943. DOI: 10.1029/2024JD042943.

Yu, W., R. Garcia, J. Yue, A. Smith, X. Wang, W. Randel, Z. Qiao, Y. Zhu, V. L. Harvey, S. Tilmes et al. (2023). 'Mesospheric temperature and circulation response to the Hunga Tonga-Hunga-Ha'apai volcanic eruption'. *J. Geophys. Res.*, 128, e2023JD039636. DOI: 10.1029/2023JD039636.

Yulaeva, E., J. R. Holton and J. M. Wallace (1994). 'On the cause of the annual cycle in tropical lower-stratospheric temperatures'. *J. Atmos. Sci.*, 51, pp. 169–174. DOI: 10.1175/1520-0469(1994)051<0169:otcota>2.0.co;2.

Zhou, X., S. S. Dhomse, W. Feng, G. Mann, S. Heddell, H. Pumphrey, B. J. Kerridge, B. Latter, R. Siddans, L. Ventress et al. (2024). 'Antarctic Vortex Dehydration in 2023 as a Substantial Removal Pathway for Hunga Tonga-Hunga Ha'apai Water Vapor'. *Geophys. Res. Lett.*, 51, e2023GL107630. DOI: 10.1029/2023gl107630.

Zhu, Y., C. G. Bardeen, S. Tilmes, M. J. Mills, X. Wang, V. L. Harvey, G. Taha, D. Kinnison, R. W. Portmann, P. Yu et al. (2022). 'Perturbations in stratospheric aerosol evolution due to the water-rich plume of the 2022 Hunga-Tonga eruption'. *Commun. Earth Environ.*, 3, 248. DOI: 10.1038/s43247-022-00580-w.

Zhuo, Z., X. Wang, Y. Zhu, W. Yu, E. M. Bednarz, E. Fleming, P. R. Colarco, S. Watanabe, D. Plummer, G. Stenchikov et al. (2025). 'Comparing multimodel ensemble simulations with observations and decadal projections of upper atmospheric variations following the Hunga eruption'. *Atmos. Chem. Phys.*, 25, pp. 13161–13176. DOI: 10.5194/acp-25-13161-2025.